NIST National Institute of Standards and Technology • U.S. Department of Commerce

Report of Test

Absolute Spectral Radiance Responsivity

of the

NASA IGA Radiometer
Model DET-8, S/N 109

Request Submitted by:

Joel McCorkle
NASA Goddard Space Flight Center
Greenbelt, MD

1. Description of Calibration Items

The device under test (DUT) consists of an indium gallium arsenide (IGA) radiance meter manufactured by L-1 Standards and Technology, Inc. (L-1), model DET-8, S/N 109 (referred to as DET-8-109) along with accessory components consisting of a temperature controller and transimpedance amplifier. The device is housed in a 2-inch diameter tube with fore-optics consisting of two apertures to form a Gershun-tube radiometer. The detector is temperature controlled (L-1 model 3100 1-L, S/N 12112) and the rear of the device has inputs for the L-1 temperature controller and a BNC output for the detector signal. Throughout the test, the temperature set point was -22.0 °C and maintained the temperature at a reading of -22.0 °C. A transimpedance amplifier (L-1 model 3300v2, S/N 020) was provided with the device and used for the calibration. Figure 1.1 shows the detector and accessory equipment as received packaged with the other NASA DET-8 radiometers (Number 106 and 107)

1.1 Calibration Request

The request was to calibrate the DUT, NASA DET-8-109, for absolute radiance responsivity from 885 nm to 1620 nm with a standard uncertainty of 0.28 % (k=1) or better.

Figure 1.1 Photographs of NASA IGA DET-8 radiometers (Numbers 106, 107, and *109*) as received. The radiometers were packaged in individual pelican cases (left) and combined in boxes with ancillary equipment consisting of the L-1 temperature controllers and transimpedance amplifiers. A new amplifier for DET-8-106 was received later, directly from the manufacturer.

2. Description of Test

The detector was characterized for absolute spectral radiance responsivity on the NIST facility for Spectral Irradiance and Radiance responsivity Calibrations using Uniform Sources (SIRCUS).[1,2] The calibration took place in various stages from Aug. 22, 2022 to Sept. 1, 2022. During each calibration test, the detector was temperature controlled at -22.0 °C by the L-1 controller and checked at the beginning and end of each calibration session. The calibration was completed from 885 nm to 1630 nm using reference detectors T-06 and DET-8-101 in overlapping ranges.

Description of laser systems used: A picosecond mode-locked (~80 MHz repetition rate) lithium triborate-optical parametric oscillator (LBO-OPO) laser was used. This laser system consists of two different cavities. Only the main cavity was used but it was used in several different ways.

1. The main cavity is designed to oscillate the signal beam and emit it through the output coupler. The output signal beam was used from 815 nm to 1060 nm.
2. When the signal beam is oscillated in the laser cavity, the idler output from the main cavity is ejected from one of the other cavity mirrors. This output of the idler beam was used from 1150 nm to 1720 nm.

3. The main cavity mirrors can also support oscillation of the idler beam when tuned through degeneracy at 1064 nm. In this situation, the idler beam is emitted through the output coupler. The laser was used in this configuration from 1070 nm to 1150 nm.

Each laser was coupled to an optical fiber connected to the side port of the integrating sphere, where the coupled laser illuminated an area toward the front of the sphere. Other optical laser components generally include a speckle-reduction device, a wavemeter, and a laser power controller.

For the LBO-OPO, the optical fiber was low-OH silica fiber and was used by both the signal and idler outputs. No speckle reduction device was employed because the laser bandwidth is broad enough to inherently reduce speckle. A Brockton Electro-Optics Corporation (BEOC) laser power controller stabilized the beam to less than the 0.1 % level using feedback from a photodiode in the sphere, removing short term as well as long term fluctuations in the power output from the various laser sources. A Bristol 621 wavemeter (S/N: 6208) was used to directly measure the vacuum wavelength of the LBO-OPO signal beam oscillated by the cavity. When the idler beam was used, the signal beam was measured by the wavemeter and converted to the corresponding idler wavelength using the relation given by equation 2.1,

$$\lambda = \frac{1}{\left(\frac{1}{\lambda_{pump}} - \frac{1}{\lambda_{signal}}\right)} \qquad (2.1)$$

where λ_{pump} is 532.2 nm and λ_{signal} is measured by the Bristol wavemeter as vacuum values. All vacuum wavelengths were subsequently converted to the air wavelength by $\lambda_{air} = \lambda_{vacuum}/n(\lambda)$, where $n(\lambda) \approx 1.00027$.

Integrating Sphere: The integrating sphere used for radiance responsivity was a LabSphere 30.48 cm (12”) diameter, Spectralon-coated sphere equipped with a 5.08 cm (2”) diameter exit aperture fabricated by LabSphere (extended-source geometry).

Data Acquisition and Control Program: The data was acquired using the LabVIEW program “SIRCUS Main Program v10.vi.” Background subtracted DC signals were sequentially collected for each detector (DUT and reference standard) along with simultaneously recorded monitor signals (also background subtracted). The collections were repeated 11 times. Each repeat sample was ratioed to the monitor signal and the average and percent standard deviation were determined.

Description of calibration detectors: The working standard reference detector T-06 (Reyer Corporation, S/N: 6) was used to measure the irradiance/radiance emitted from the source sphere from 815 nm to 995 nm. It is a 5-element, tunnel-trap detector equipped with an aperture having an area of 9.985 mm^2. The T-06 irradiance responsivity was calibrated by combining a calibration of the power responsivity with a calibration of the aperture area. The power responsivity was completed by NIST Primary Optical Watt Radiometer (POWR)[3] in 2016[4] and the aperture was calibrated by the NIST aperture area facility[5] in Mar. 2023.[6] Standard reference detector T-06 was connected to the transimpedance preamplifier Femto SIRCUS 12 (DPLCA-200, S/N: 01-41-1435) with a gain setting that has been previously calibrated.[7,8] The nominal gain setting was 10^6 V/A for all measurements and the switch settings were L, DC, FBW, and GND.

A second standard reference detector, NIST SIRCUS DET-8-101, was used for the range 885 nm to 1630 nm. This reference detector is the same model radiometer as the DUT but has been

calibrated for radiance responsivity against the NIST SIRCUS Pyro #2 irradiance meter.[9] This detector used current-to-voltage converter (CVC) SIRCUS Precision CVC (S/N: 2).[10] The gain setting was 10^6 V/A for all measurements. This detector also used an L-1 temperature controller (model 3100) which maintained the temperature at -19.0 °C with the setpoint at -19.0 °C. The most recent calibration of this detector was performed after the measurements for the DUT were made but was applied to the analysis of the DUT responsivity.

The monitor detector was a silicon or an IGA photodiode mounted directly to the source sphere. It was connected to a Stanford Research Systems current preamplifier (Model SR570, S/N: 57687).

3-axis stage: The integrating sphere is mounted on an XYZ translation stage, with the Z-position (along the optical axis) measured with a linear encoder. The X- and Y-axes enable the source to be properly positioned in front of an instrument before it measures the sphere radiance. The Z-position is used to accurately determine the separation between relevant apertures.

Measurement Setup: Detectors used in these experiments were mounted to tip-tilt stages and aligned to the optical axis of the integrating sphere source using a double-headed laser. To align the detectors to the sphere, the double-headed laser was first mounted in-front of the large sphere where one end of the laser was previously aligned to the center of the sphere aperture. The other end of the laser was retroreflected from a glass microscope slide on each detector to align to the optical axis. Lastly, the laser was centered on each detector using the 3-axis stage to determine the X, Y position. See Figure 2.1 for photographs of the measurement setup and temperature controller setup. This calibration was performed simultaneously with other test detectors as shown.

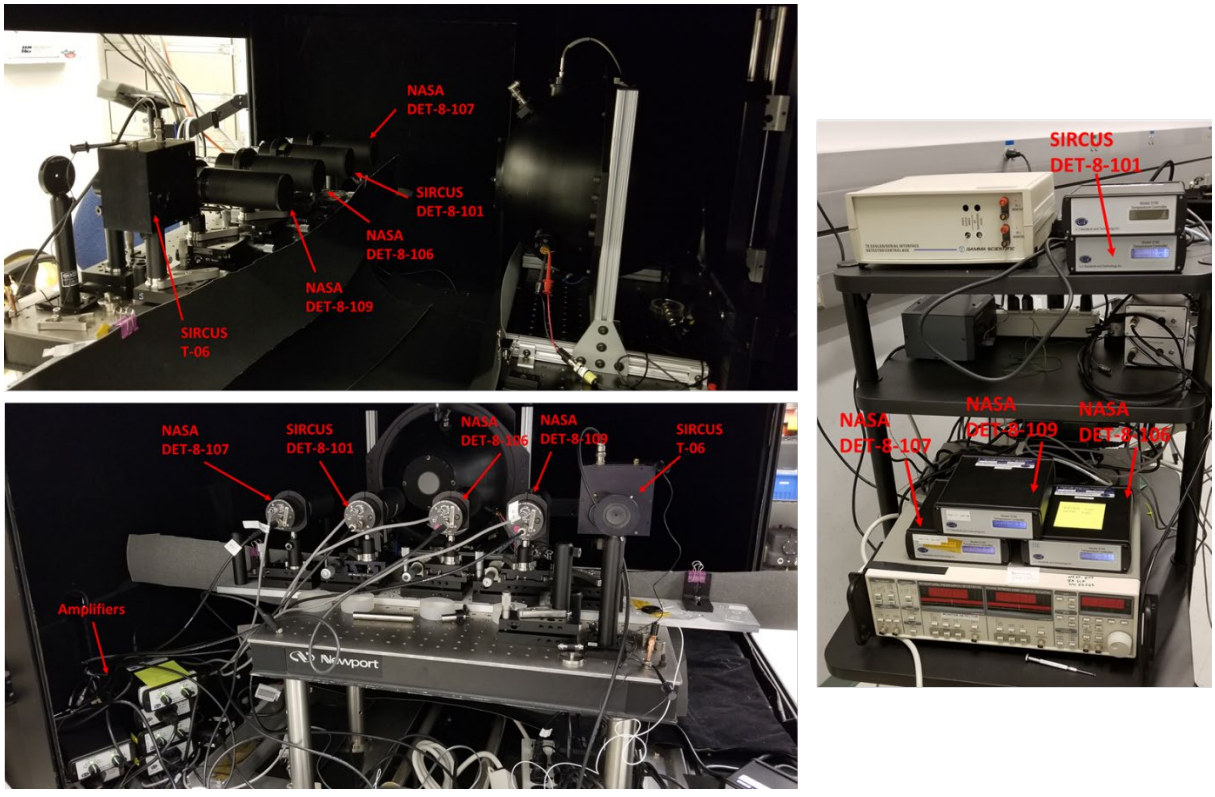

Figure 2.1 Photographs of the detector setup inside the SIRCUS enclosure (left) and temperature controller setup (right).

2.1 Radiance Responsivity of NASA IGA DET-8-109 from T-06 and DET-8-101

Absolute radiance responsivity measurements were completed for DUT DET-8-109 versus the standard reference detectors T-06[4,6] and DET-8-101[9] from 885 nm to 1630 nm using the SIRCUS facility. The DUT was supplied with an associated transimpedance preamplifier without known calibration of the gain settings. Therefore the DUT was calibrated together with the preamplifier to yield radiance responsivity units of [V/(W/cm^2 sr)], where the nominal gain setting was 10^6 V/A (multiplier = 1) for all measurements.

The integrating sphere source was the 12" diameter sphere described in Section 2 with a 5.08 cm (2") aperture but the sphere was placed at different positions depending on the reference detector. A fixed position Z = 62.065 mm relative to both the DUT and the reference detector was used for measurements versus DET-8-101. This placed the sphere approximately 28 cm from the DUT and reference DET-8-101 apertures, as measured by a Mitutoyo ruler, and placed the field of view completely within the 2-inch diameter sphere output aperture. Response maps for the DUT, both in the X,Y aperture plane and along the optical Z-axis, were also measured, verifying the central position and underfilled configuration of the DUT relative to the sphere aperture. Using DET-8-101 allowed for a direct radiance-to-radiance scale transfer and eliminated the distance contribution to the uncertainty typically present when irradiance meter standard reference detectors are used.

For the calibration against reference trap T-06, an irradiance meter, the sphere was moved to different positions for measurement of the DUT and reference trap detector. The sphere was placed the same as above (Z = 62.065 mm) for measurement of the DUT, but this position would overfill the individual photodiodes comprising the trap detectors, leading to an erroneous loss of irradiance signal. Therefore, the stage was instead moved to Z = 300.374 mm for measurement of T-06 to establish the sphere source radiance. This position placed the sphere aperture well within the acceptance angle of the reference detector as suggested in Section 3.1, below. The working distance was determined for T-06 (61.117 cm) from the sphere Z-position and the radiometrically determined detector position, as described in Section 3.2 below.

3. Results of Test

For this calibration, a radiance calibration measurement was performed using two different reference detectors. The reference detectors (trap T-06 or DET-8-101) established the radiance emitted from the source sphere. For DET-8-101, the radiance of the source was determined directly from the previously calibrated radiance responsivity. Even though T-06 is an irradiance meter, it was also used to determine the source radiance, requiring knowledge of the solid angle of the source. To determine the solid angle, the distance between the reference detector aperture and the integrating sphere source aperture was measured, along with the integrating sphere and trap aperture areas: See Section 3.1. The reference detector T-06 position was determined radiometrically, as described in Section 3.2, and the distance from the source was determined by measuring the Z-position with the linear encoder on the Z-axis stage.

3.1 Determination of the sphere source radiance for irradiance meter reference detectors

The radiance of the sphere source was determined with the flux transfer method for the calibration against the trap irradiance meter T-06. Radiant power was measured from the sphere source passing through two precision apertures, one on the source sphere and the other on the reference

trap detector T-06. The radiance L [W m^{-2} sr^{-1}] of the sphere was determined from radiant power P [W] and the geometric extent G by:

$$L = \frac{P}{G} \tag{3.1}$$

The geometric extent G [m^2 sr] is given by

$$G = \frac{\pi^2}{2}\left[(s^2 + r_s^2 + r_D^2) - \{(s^2 + r_s^2 + r_D^2)^2 - 4r_s^2 r_D^2\}^{1/2}\right] \tag{3.2}$$

where r_S is the radius of the aperture in front of the source, r_D is the radius of the aperture in front of the reference detector, and s is the distance between the two apertures. The diameter of the sphere aperture was large enough (50.8 mm) to overfill the radiance measurement angle of the DUT radiometer by the sphere output radiation. The distance, s, was chosen large enough so that the sphere aperture was well within the acceptance angle of reference detector T-06.

3.2 Detector offset and offset uncertainty determination for irradiance meters

For radiance measurements using an irradiance meter reference, knowledge of the distance between the source and the reference detector aperture is required. That distance for reference T-06 was determined radiometrically. At several different Z positions, the detector and monitor voltages were recorded to yield a relative irradiance. Using the $1/Z^2$ law for on-axis irradiance (inverse square law) the resultant data can be fit by a point-source geometry (Equation 3.3) and an extended-source geometry (the experimental configuration, Equation 3.4) to yield the Z-position of the detector aperture plane. From the Z-position encoder reading used in the radiance or irradiance responsivity measurements and the detector Z-position from the radiometric $1/Z^2$ law fit, the actual detector aperture to sphere aperture distance in millimeters (working distance) was determined. Figure 3.1 is a schematic of the configuration.

The inverse square law fitting equation for a point-source geometry is:

$$y = \frac{m_1}{(M_0 - m_2)^2} \tag{3.3}$$

Where y is the relative irradiance, m_1 is a fitting constant, M_0 is Z-position of the integrating sphere that is read by the Z-encoder, and m_2 is the Z-position of zero offset between the two apertures. The fitting uncertainty in m_2, for the sphere position during calibration, gives the uncertainty in the distance between the two apertures.

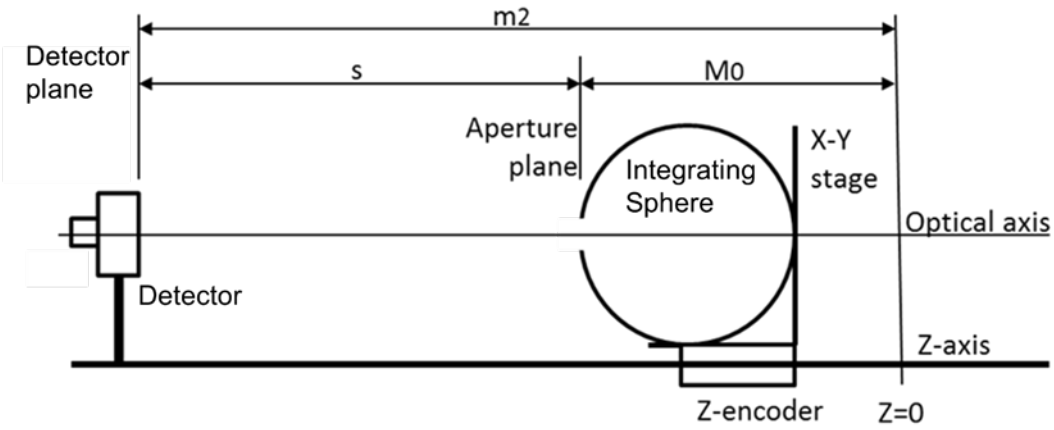

Figure 3.1. Schematic of the configuration for determining detector-sphere distance radiometrically for an irradiance meter. Here the detector is the reference T-06.

If the source aperture is large, the non-point source geometry expression is fit to the data:

$$y = \frac{m_1}{((M_0 - m_2)^2 + m_3^2 + m_4^2)} \qquad (3.4)$$

where y, m_1, M_0, and m_2 are the same as in Eq. 3.3. $m_3 = r_d$, the radius of the detector aperture, and $m_4 = r_s$, the radius of the integrating sphere aperture. Equation 3.4 is valid in the limit where

$$(r_s^2 + r_d^2 + s^2) \gg 2r_s r_d \qquad (3.5)$$

and s is the distance between the source and detector apertures. The inverse square law measurements along with the fit of equation 3.4 to the data for the reference detector can be seen in Figure 3.2, below. At a separation, s, equal to the working distance, the ratio given by equation 3.5 was determined for each irradiance detector. This result is summarized in Table 3.1 and shows the condition of equation 3.5 holds and that equation 3.4 is valid in each case. The residuals are approximately 3 orders of magnitude smaller than the base measurement and show there is no obvious bias or offset. The fitting results are also summarized in Table 3.2.

Table 3.1 Results of equation 3.5 at minimum separation distances.

Detector	r_s (cm)	r_d (cm)	s (cm)	Ratio (Eq 3.5)
T-06	2.54	0.178	61.117	4197.9

Table 3.2 Results of the inverse square law fits of equation 3.4 to the data.

Detector	m_2 (mm)	Fitting Uncertainty (mm) (k=1)	R, fit
T-06	-310.8	0.075	1

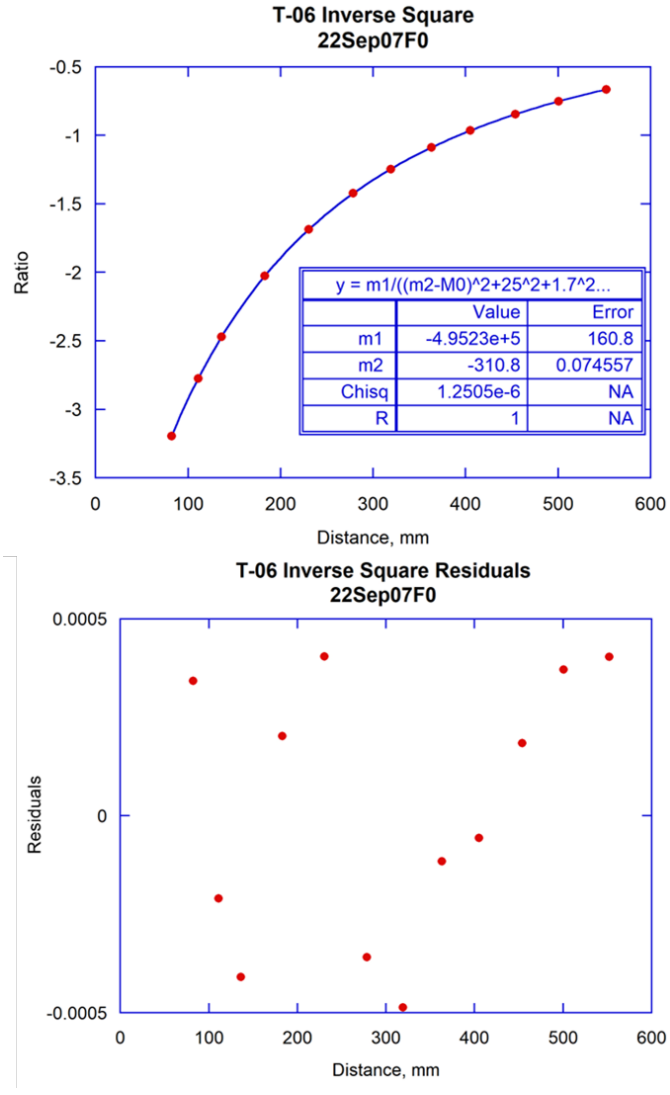

Figure 3.2 Offset and uncertainty fit of the extended-source geometry equation 3.4 to the irradiance response data (top) and residuals from the fit (bottom) for distance determination of T-06.

3.3 Absolute Spectral Radiance Responsivity of NASA IGA DET-8-109

Absolute spectral radiance responsivity of NASA IGA DET-8-109 was measured from 885 nm to 1630 nm using two standard reference detectors (T-06 and DET-8-101) in overlapping spectral ranges. This result is shown in Figure 3.3 and the individual data points are provided in Table 3.3. An expanded view of the overlap region is displayed by the bottom plot in Figure 3.3 and shows good agreement between the radiance responsivity result derived from each reference detector. Error bars are included in the plots but are smaller than the size of the points in some cases and difficult to observe on the plotted Y-axis scale. Figure 3.4 plots the percent difference between the radiance responsivity derived from each reference detector. At each point in the overlap region, the percent difference is 0.15% or less, which is smaller than the k=2 uncertainty.

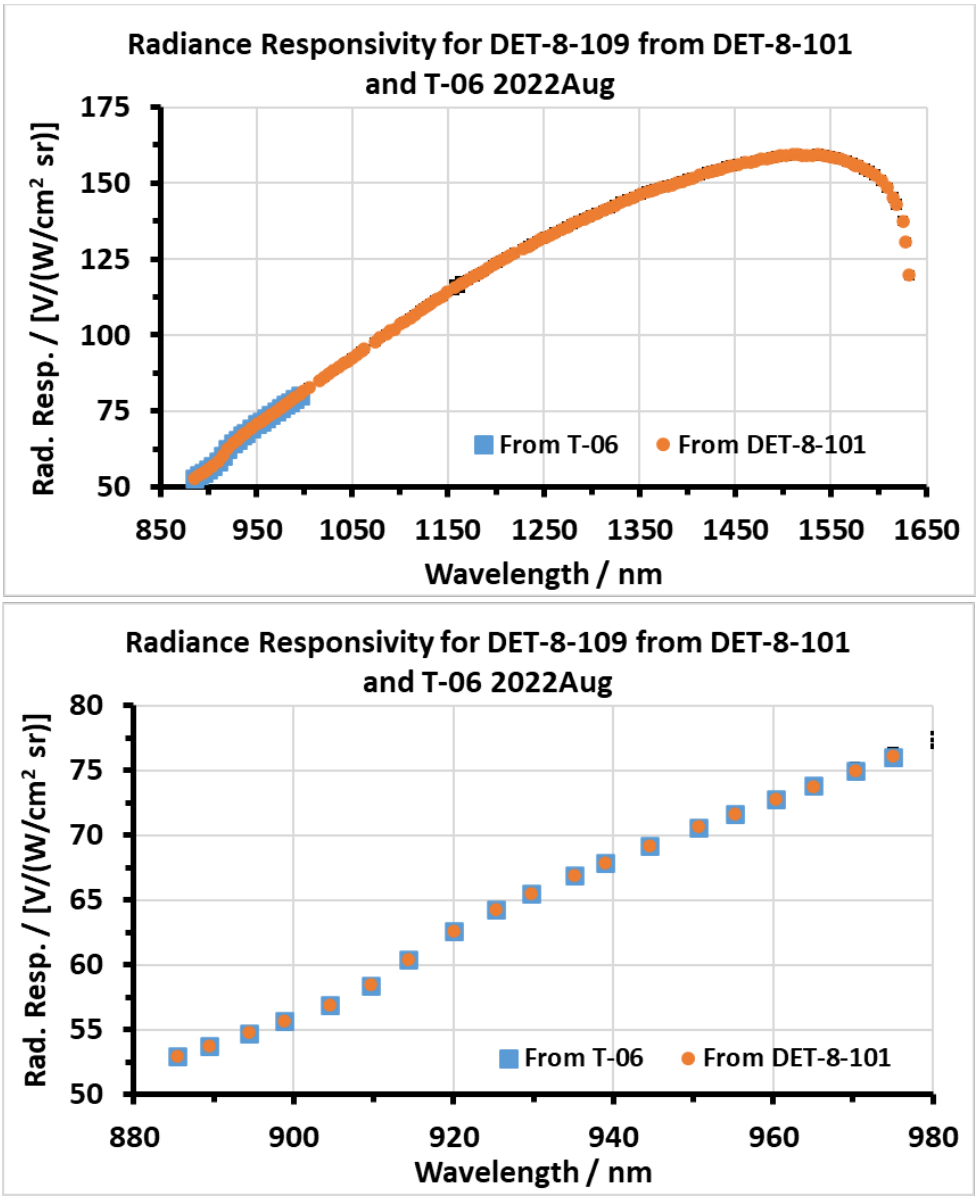

Figure 3.3 Absolute spectral radiance responsivity of DET-8-109 from DET-8-101 (orange circles) and T-06 (blue squares) over the full spectral range (top) and in the overlap region (bottom).

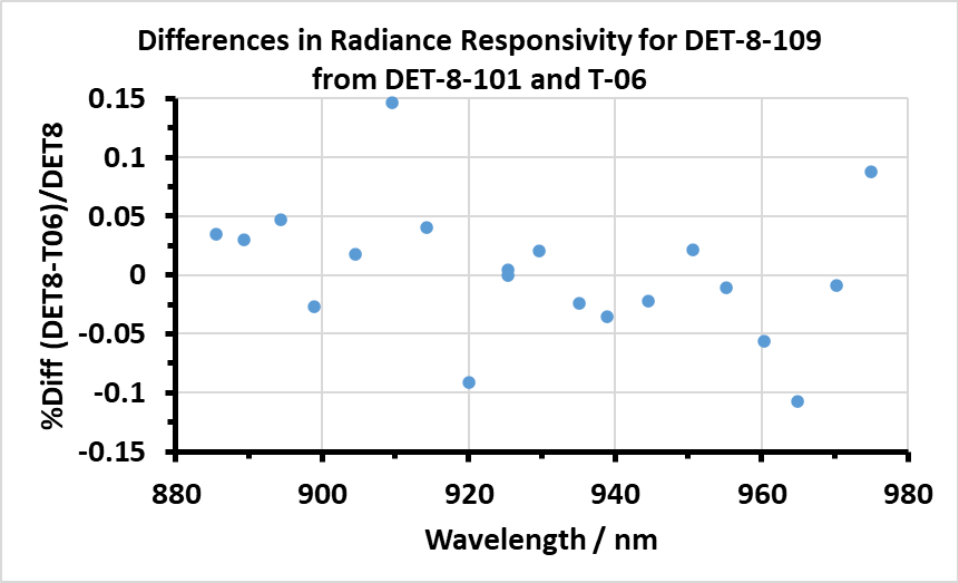

Figure 3.3 Percent difference between the absolute spectral radiance responsivity of DET-8-109 from DET-8-101 and T-06.

Table 3.3 Tabulated absolute spectral radiance responsivity data for NASA IGA DET-8-109.

Reference Detector	Wavelength [nm]	Radiance Responsivity [V/(W/cm² sr)]	Total Percent Uncertainty [k=1]
T-06	885.45	5.2945E+01	0.07
T-06	889.38	5.3744E+01	0.07
T-06	894.35	5.4723E+01	0.07
T-06	898.87	5.5658E+01	0.07
T-06	904.45	5.6881E+01	0.07
T-06	909.60	5.8367E+01	0.07
T-06	914.27	6.0364E+01	0.07
T-06	920.06	6.2633E+01	0.08
T-06	925.36	6.4295E+01	0.08
T-06	929.67	6.5515E+01	0.08
T-06	935.10	6.6919E+01	0.08
T-06	938.95	6.7857E+01	0.08
T-06	944.50	6.9200E+01	0.08
T-06	950.66	7.0611E+01	0.08
T-06	955.20	7.1651E+01	0.08
T-06	960.35	7.2799E+01	0.09
T-06	964.98	7.3822E+01	0.10
T-06	970.24	7.4965E+01	0.10

T-06	974.97	7.6010E+01	0.11
T-06	980.34	7.7123E+01	0.13
T-06	984.57	7.7981E+01	0.14
T-06	990.05	7.9136E+01	0.15
T-06	994.98	8.0180E+01	0.16
DET-8-101	885.45	5.2963E+01	0.12
DET-8-101	889.38	5.3760E+01	0.12
DET-8-101	894.35	5.4748E+01	0.12
DET-8-101	898.87	5.5643E+01	0.12
DET-8-101	904.45	5.6891E+01	0.12
DET-8-101	909.60	5.8452E+01	0.12
DET-8-101	914.27	6.0388E+01	0.12
DET-8-101	920.06	6.2576E+01	0.12
DET-8-101	925.36	6.4298E+01	0.12
DET-8-101	929.67	6.5529E+01	0.12
DET-8-101	935.10	6.6903E+01	0.12
DET-8-101	938.95	6.7833E+01	0.12
DET-8-101	944.50	6.9185E+01	0.12
DET-8-101	950.66	7.0626E+01	0.12
DET-8-101	955.20	7.1644E+01	0.12
DET-8-101	960.35	7.2758E+01	0.14
DET-8-101	964.98	7.3742E+01	0.35
DET-8-101	970.24	7.4958E+01	0.35
DET-8-101	974.97	7.6077E+01	0.35
DET-8-101	980.34	7.7311E+01	0.35
DET-8-101	985.18	7.8300E+01	0.35
DET-8-101	990.05	7.9353E+01	0.35
DET-8-101	994.99	8.0412E+01	0.35
DET-8-101	999.34	8.1521E+01	0.35
DET-8-101	1004.99	8.2899E+01	0.33
DET-8-101	1015.19	8.4900E+01	0.33
DET-8-101	1020.36	8.5960E+01	0.33
DET-8-101	1024.93	8.7070E+01	0.33
DET-8-101	1030.22	8.8284E+01	0.33
DET-8-101	1035.57	8.9382E+01	0.33
DET-8-101	1040.97	9.0433E+01	0.33
DET-8-101	1045.05	9.1478E+01	0.33
DET-8-101	1049.85	9.2590E+01	0.33
DET-8-101	1055.41	9.3784E+01	0.33
DET-8-101	1059.61	9.4776E+01	0.33
DET-8-101	1062.46	9.5416E+01	0.34
DET-8-101	1073.89	9.7772E+01	0.33
DET-8-101	1078.91	9.9049E+01	0.33

DET-8-101	1085.50	1.0044E+02	0.33
DET-8-101	1089.95	1.0144E+02	0.33
DET-8-101	1093.67	1.0195E+02	0.33
DET-8-101	1100.53	1.0374E+02	0.34
DET-8-101	1104.40	1.0453E+02	0.33
DET-8-101	1110.50	1.0576E+02	0.33
DET-8-101	1115.07	1.0683E+02	0.33
DET-8-101	1121.38	1.0824E+02	0.33
DET-8-101	1124.54	1.0892E+02	0.34
DET-8-101	1128.53	1.0974E+02	0.33
DET-8-101	1131.82	1.1049E+02	0.33
DET-8-101	1136.53	1.1157E+02	0.34
DET-8-101	1138.93	1.1192E+02	0.33
DET-8-101	1144.38	1.1277E+02	0.35
DET-8-101	1149.31	1.1412E+02	0.34
DET-8-101	1156.79	1.1569E+02	0.88
DET-8-101	1162.68	1.1673E+02	0.88
DET-8-101	1166.06	1.1733E+02	0.39
DET-8-101	1171.19	1.1825E+02	0.39
DET-8-101	1177.21	1.1929E+02	0.39
DET-8-101	1181.55	1.2008E+02	0.39
DET-8-101	1186.81	1.2100E+02	0.33
DET-8-101	1192.11	1.2202E+02	0.33
DET-8-101	1197.46	1.2318E+02	0.33
DET-8-101	1201.06	1.2381E+02	0.33
DET-8-101	1205.57	1.2462E+02	0.33
DET-8-101	1211.04	1.2561E+02	0.33
DET-8-101	1214.74	1.2622E+02	0.33
DET-8-101	1219.34	1.2710E+02	0.33
DET-8-101	1228.71	1.2842E+02	0.33
DET-8-101	1234.41	1.2932E+02	0.33
DET-8-101	1238.23	1.3006E+02	0.33
DET-8-101	1244.00	1.3108E+02	0.33
DET-8-101	1247.88	1.3162E+02	0.33
DET-8-101	1251.80	1.3226E+02	0.33
DET-8-101	1256.71	1.3290E+02	0.33
DET-8-101	1261.65	1.3373E+02	0.33
DET-8-101	1268.67	1.3479E+02	0.33
DET-8-101	1274.73	1.3571E+02	0.33
DET-8-101	1279.83	1.3656E+02	0.33
DET-8-101	1286.01	1.3747E+02	0.33
DET-8-101	1292.24	1.3832E+02	0.33
DET-8-101	1296.41	1.3883E+02	0.33

DET-8-101	1299.58	1.3932E+02	0.33
DET-8-101	1305.93	1.4022E+02	0.33
DET-8-101	1312.35	1.4107E+02	0.33
DET-8-101	1318.84	1.4183E+02	0.33
DET-8-101	1324.29	1.4275E+02	0.33
DET-8-101	1330.88	1.4385E+02	0.33
DET-8-101	1337.54	1.4458E+02	0.33
DET-8-101	1344.29	1.4533E+02	0.33
DET-8-101	1351.09	1.4627E+02	0.33
DET-8-101	1357.96	1.4716E+02	0.33
DET-8-101	1362.58	1.4767E+02	0.33
DET-8-101	1366.07	1.4798E+02	0.33
DET-8-101	1371.91	1.4852E+02	0.33
DET-8-101	1379.00	1.4915E+02	0.33
DET-8-101	1383.77	1.4954E+02	0.33
DET-8-101	1388.56	1.5007E+02	0.33
DET-8-101	1394.60	1.5069E+02	0.33
DET-8-101	1400.69	1.5136E+02	0.33
DET-8-101	1405.61	1.5179E+02	0.33
DET-8-101	1413.04	1.5260E+02	0.33
DET-8-101	1420.57	1.5345E+02	0.33
DET-8-101	1425.62	1.5387E+02	0.33
DET-8-101	1430.71	1.5421E+02	0.33
DET-8-101	1435.85	1.5478E+02	0.33
DET-8-101	1441.02	1.5532E+02	0.33
DET-8-101	1446.22	1.5576E+02	0.33
DET-8-101	1452.77	1.5632E+02	0.33
DET-8-101	1460.71	1.5683E+02	0.33
DET-8-101	1466.07	1.5706E+02	0.33
DET-8-101	1471.45	1.5744E+02	0.33
DET-8-101	1476.86	1.5784E+02	0.33
DET-8-101	1482.32	1.5804E+02	0.33
DET-8-101	1487.85	1.5836E+02	0.33
DET-8-101	1493.37	1.5872E+02	0.33
DET-8-101	1497.55	1.5895E+02	0.33
DET-8-101	1503.16	1.5904E+02	0.33
DET-8-101	1510.24	1.5937E+02	0.33
DET-8-101	1514.52	1.5951E+02	0.33
DET-8-101	1520.29	1.5920E+02	0.33
DET-8-101	1524.62	1.5912E+02	0.33
DET-8-101	1530.45	1.5910E+02	0.33
DET-8-101	1536.31	1.5945E+02	0.33
DET-8-101	1542.23	1.5920E+02	0.33

DET-8-101	1548.17	1.5871E+02	0.33
DET-8-101	1554.17	1.5848E+02	0.33
DET-8-101	1560.23	1.5785E+02	0.33
DET-8-101	1566.31	1.5721E+02	0.33
DET-8-101	1572.46	1.5669E+02	0.33
DET-8-101	1575.54	1.5595E+02	0.33
DET-8-101	1578.65	1.5567E+02	0.33
DET-8-101	1584.90	1.5470E+02	0.33
DET-8-101	1589.62	1.5388E+02	0.33
DET-8-101	1595.95	1.5269E+02	0.33
DET-8-101	1602.33	1.5084E+02	0.33
DET-8-101	1608.76	1.4848E+02	0.33
DET-8-101	1615.24	1.4530E+02	0.33
DET-8-101	1618.49	1.4304E+02	0.33
DET-8-101	1625.05	1.3746E+02	0.33
DET-8-101	1628.36	1.3068E+02	0.33
DET-8-101	1631.67	1.1967E+02	0.33

3.4 Uncertainty Analysis for the Radiance Responsivity of NASA IGA DET-8-109

The uncertainty analysis for DET-8-109 is shown in Table 3.4 and includes the typical uncertainty components. Components for measurement standard deviation and the reference detector irradiance calibrations displayed in the table are averaged over all the wavelengths. Uncertainties at individual wavelengths can be taken from the data tables and are provided in the calibration files. The calibration from the reference detector DET-8-101 doesn't include typical components for distance or aperture area because it is a radiance-to-radiance transfer in this case. For the calibration from DET-8-101, there is an additional uncertainty component for the reference detector position. DET-8-101 was placed with 28 cm distance away from the sphere aperture during these measurements whereas it was re-calibrated later with the sphere 32 cm away. The component Reference DET-8-101 Position accounts for the error associated with the different aperture separation.

Table 3.4 Uncertainty Budget for Absolute Spectral Radiance Responsivity of DET-8-109.

	Relative Standard k=1 Uncertainty [%]		
Uncertainty Component	**From T-06: 885 nm to 995 nm**	**From DET-8-101 885 nm to 960 nm**	**From DET-8-101 965 nm to 1630 nm**
Reference Detector Responsivity Calibration.[1]	0.06	0.09	0.33
Measurement Standard Deviation[2]	0.002	0.002	0.012
Reference Detector Distance[3]	0.024	N.A.	N.A.
Geometry Alignment	0.05	0.05	0.05
Amplifier Gain	0.01	0.01	0.01
Aperture Areas	0.03	N.A.	N.A.
Wavelength	0.03	0.03	0.03
Reference DET-8-101 Position	N.A.	0.05	0.05
Combined Standard Uncertainty[4]	**0.09**	**0.12**	**0.34**

Note 1: This is the reference detector responsivity averaged over all the wavelengths. T-06 responsivity uncertainty increases towards 1000 nm but is less than 0.05 % below 950 nm. DET-8-101 responsivity uncertainty is higher at wavelengths longer than 965 nm where the responsivity comes from SIRCUS Pyro #1.
Note 2: This is the combined measurement percent standard deviation for the DUT and reference detector averaged across the entire range. Values for individual wavelengths are provided in the calibration file.
Note 3: Percent uncertainty in the distance for the reference irradiance detector, including an additional factor of 2 as irradiance depends on the distance squared. There is no contribution from the DUT because it is a radiance meter. There is no distance uncertainty when the reference detector is DET-8-101 because it and the DUT are both radiance meters.
Note 4: This is not the full calibration uncertainty budget. The uncertainty budget, Table 3.4, does not include environmental effects on both the reference detector and the DUT radiometer. No evaluations of instrument performance characteristics such as temperature dependence, response linearity or temporal stability were performed. For estimates in the interpolated uncertainty, see the reference.[11]

4. General Information

Information was recorded in the SIRCUS Vis #21 laboratory notebook, pp.131-139.

The calibration measurements, data analysis, and report writing were performed by Brian G. Alberding.

This calibration required 8 days of laboratory work (including setup, troubleshooting, and data

collection) on SIRCUS and 7 days of data reduction, analysis, and reporting.

Significant experimental notes:

1. Reference detector calibrations have changed in several ways since NASA IGA detectors were calibrated from T-06 and DET-8-101. The recalibrations of the reference detector responsivity were done after the measurements reported here were completed. The new reference detector responsivities were used to reanalyze the DUT responsivity.
    a. The trap apertures have been recalibrated by the NIST Aperture Area Measurement Facility. The trap aperture area only changed by approximately 0.02 percent.
    b. The DET-8-101 calibration changed significantly compared to prior NASA detector calibrations due to its heritage from SIRCUS Pyro #1 as detailed elsewhere.[12] We could consider, re-analyzing data from previous instances of NASA calibrations that used DET-8-101 or SIRCUS Pyro #1 as the reference detector.
2. A grounding wire was added to the DET-8-109 amplifier from the voltage out connector to the optical table.
3. There were several instances where the DET-8-109 signal dropped relative to the other detectors and the sphere monitor signal. The measurements were repeated in these instances and the signal appeared normal. Measurements where the signal dropped out were excluded from the responsivity analysis.
4. A response map along the optical Z-axis was measured for the DUT and is displayed in Figure 4.1. This can be used to account for differences that arise from placing the DUT at a sphere offset position in future calibrations that is different from which it was calibrated here.

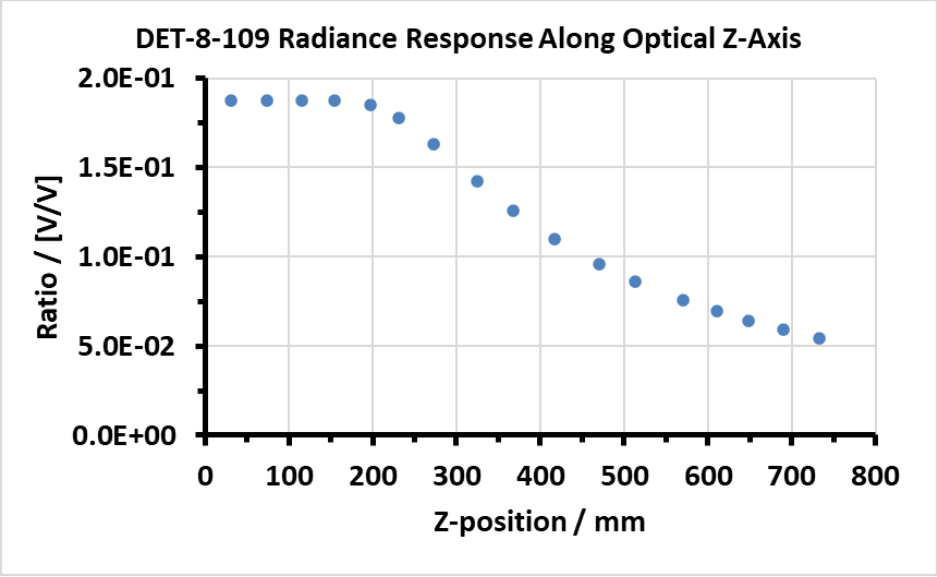

Figure 4.1 Response map (where the vertical axis is the ratio of the DUT signal to sphere monitor signal) along the optical Z-axis for DET-8-109.

Information about data files:

1. Full data files for the radiance responsivity of DET-8-109 are located on Elwood under:

\\cfs2e.nist.gov\685\internal\G04\SIRCUS\SIRCUS\Calibrations\SIRCUS Calibrations\FY2022 Calibrations\GLAMR InGaAs Special\After REF DET-8-101 ReCal

Data file for the radiance responsivity of DET-8-109: "Combined Results NASA IGA DET-8-109 after Ref ReCal.xlsx"

The files located in these directories are meant for internal NIST use only. Please do not distribute without authorization.

References

1. Brown, S. W., Eppeldauer, G. P. & Lykke, K. R. "Facility for spectral irradiance and radiance responsivity calibrations using uniform sources." *Appl. Opt.,* **45**, 8218–8237 (2006).
2. Woodward, J. T. *et al.* "Invited Article: Advances in tunable laser-based radiometric calibration applications at the National Institute of Standards and Technology, USA." *Review of Scientific Instruments* **89**, 091301 (2018).
3. Houston, J. M. & Rice, J. P. "NIST reference cryogenic radiometer designed for versatile performance." *Metrologia* **43**, S31–S35 (2006).
4. Shaw, P.-S. "Report of Calibration for SIRCUS Si Trap Detectors T06 and T04 from 475 nm to 1000 nm." (2016).
5. Fowler, J. & Litorja, M. "Geometric area measurements of circular apertures for radiometry at NIST." *Metrologia* **40**, S9–S12 (2003).
6. Griesmann, U. "Report of Calibration of Aperture Area Measurement (39200S) for Three Circular Apertures (Reyer Trap T-01, T-04, and T-06)," Order Item No.: O-0000047647. (2023).
7. Larason, T. & Miller, C. C. "Gain Calibration of Current-to-Voltage Converters." *J. RES. NATL. INST. STAN.* **123**, 123019 (2018).
8. Larason, T. C. "Special Test of Current-to-Voltage Converters (39300S) for FEMTO DLPCA-200 No. 01-41-1435," Order Item No: O-0000036360. (2022).
9. Alberding, B. G. "Report of Test: Absolute Spectral Radiance Responsivity of the NIST IGA Detector DET-8-101," 685.04/SRS2023-002. (2023).
10. Larason, T. C. "Special Test of Current-to-Voltage Converters (39300S) for Precision CVC No. 2," Order Item No: O-0000036360. (2022).
11. Gardner, J. L. "Uncertainties in Interpolated Spectral Data." *J. Res. Natl. Inst. Stand. Technol.* **108**, 69–78 (2003).
12. Alberding, B. G. "Report of Test: Absolute Spectral Irradiance Responsivity of the Pyroelectric Detector SIRCUS Pyro #1," 685.04/SRS2023-001. (2023).

Distribution Restrictions: None

Tabulated calibration data files were provided along with this report.
Filename: "DET-8-109_RadResp_FY2022_Final.xlsx"

Prepared by:

BRIAN ALBERDING

Digitally signed by BRIAN ALBERDING
Date: 2023.04.27 13:25:27 -04'00'

Brian G. Alberding
Remote Sensing Group
Sensor Science Division
Physical Measurement Laboratory
(301) 975-4664

Approved by:

JOSEPH RICE

Digitally signed by JOSEPH RICE
Date: 2023.04.29 06:54:07 -04'00'

Joseph P. Rice, Leader
Remote Sensing Group
Sensor Science Division
Physical Measurement Laboratory
(301) 975-2133